Disentangling Diagenesis From the Rock Record: An Example From the Permo-Triassic Wordie Creek Formation, East Greenland

J. Roberts[1,2] (iD), **A. V. Turchyn[1]** (iD), **P. B. Wignall[3]** (iD), **R. J. Newton[3]** (iD), **and C. H. Vane[4]** (iD)

[1]Department of Earth Sciences, University of Cambridge, Downing Street, Cambridge, United Kingdom, [2]Now at Alfred-Wegener-Institut Helmholtz-Zentrum für Polar- und Meeresforschung, Bremerhaven, Germany, [3]School of Earth and Environment, University of Leeds, Leeds, United Kingdom, [4]British Geological Survey, Keyworth, United Kingdom

Abstract The measurement of isotope ratios in sedimentary rocks deposited over geological time can provide key insights to past environmental change over important intervals in the past. However, it is important to be aware that secondary alteration can overprint the original isotopic records. We demonstrate this principle using high-resolution carbon, sulfur, and oxygen isotope measurements in organic carbon, pyrite, and carbonate minerals ($\delta^{13}C_{org}$, $\delta^{34}S_{pyr}$, $\delta^{34}S_{CAS}$, $\delta^{13}C_{carb}$, and $\delta^{18}O_{carb}$) and kerogen analyses (HI and OI) from the Wordie Creek Formation, East Greenland. These sediments were initially deposited across the Permo-Triassic transition, but as we will show, the carbonate record has been altered by interaction with meteoric water significantly after initial deposition. Comparison of the better preserved organic carbon and pyrite records with a proximal Permo-Triassic sequence reveals significant pyrite-sulfur isotope variability across the Permo-Triassic transition. This regional heterogeneity argues against basin-wide euxinia and instead suggests localized changes in sulfur fractionation in response to variations in organic carbon flux. This hypothesis can be used to explain seemingly inconsistent regional trends in other sulfur isotopes across the Permo-Triassic transition.

Plain Language Summary Much of what is known about environmental change in the past has been determined through measuring the chemical properties of rocks. In this study, we demonstrate how those chemical properties may have been altered by processes occurring millions of years later. We show new chemical records from rocks deposited during across the Permo-Triassic boundary (the world's largest mass extinction event) in East Greenland and discuss how some of the records have been altered by interaction with rain water millions of years after they were deposited. Finally, we talk about the records that have been unaffected by alteration, and what they imply for environmental changes occurring across the Permo-Triassic boundary.

1. Introduction

Geochemical records preserved in the geological record provide key information on past environmental changes. In particular, stable carbon isotopes (^{12}C and ^{13}C) can be used to understand the large-scale changes in the global carbon cycle over intervals of significant ecological upheaval. For example, a global negative carbon isotope excursion coincident with the Permo-Triassic mass extinction has been suggested to reflect either the collapse of marine productivity (Looy et al., 2001; Nabbefeld et al., 2010) and/or the injection of ^{13}C-depleted carbon to the atmosphere and oceans (Korte & Kozur, 2010; Payne & Clapham, 2012). While geochemical records provide important constraints on environmental change occurring in the past, it is important to be aware of processes that have the potential to affect the fidelity of these geochemical archives. Carbonate minerals are particularly prone to postdepositional alteration, with the potential for recrystallization to reset the original isotopic signatures during burial or exhumation of the sequence. The isotopic composition of the carbonate can be used to infer the extent of the postdepositional diagenesis of the carbonate phase and the source of any secondary fluid (Swart, 2015).

In this study, we measure carbon and sulfur isotopes on various organic and inorganic phases within a Permo-Triassic succession from East Greenland. The isotopic signatures of these phases reveal that the carbonate minerals have been recrystallized. We use a simple water-rock interaction model to infer the timing

of alteration of the carbonate phase at these sites. We then go on to discuss the geochemical records that we infer to be unaltered by secondary alteration and discuss the implication of these records for environmental change across the Permo-Triassic boundary.

2. Geological Setting

The Permian-Triassic sequences of the Jameson Land Basin were deposited during a time of active faulting and subsidence that resulted in some of the thickest sequences of uppermost Permian/lower Triassic strata globally (Stemmerik et al., 2001). In this region, the Late Permian Schuchert Dal Formation is overlain by the Early Triassic Wordie Creek Formation (Wignall & Twitchett, 2002b). The sedimentary environment has been interpreted to be a deep marine, syn-rift basin where thick fan-delta sandstones and conglomerates interleave with basinal mudstones and small turbidite lobes (Wignall & Twitchett, 2002b). In shale-dominated sections, the end-Permian mass extinction is seen to occur at the sharp transition from burrowed, silty mudstones of the Schuchert Dal Formation to laminated, pyritic shales at the base of the Wordie Creek Formation.

Previous geochemical studies spanning the Permo-Traissic boundary in the Jameson Land Basin have focused on the Schuchert Dal valley (also referred to as the Fiskegrav section; Fenton et al., 2007; Nielsen et al., 2010; Stemmerik et al., 2001; Twitchett et al., 2001), 100 km south of the Oksedal sections studied here (Figure 1). The cliff sections labeled OK1–4 in Wignall and Twitchett (2002a) were sampled at irregular intervals. In this study, geochemical measurements have been performed on sections OK1, OK2, and OK4. The sections OK1 and OK2 are located less than 500 m apart, whereas OK4 is slightly more distal (3 km from OK1 and OK2).

Out of the three Oksdal sections studied here, OK4 represents the most complete section spanning the Permo-Triassic transition. The two most eastern sections, OK1 and OK2 both have a coarse grained sandstone unit at their base, which has been interpreted to be a submarine channel infill (Wignall & Twitchett, 2002b; Figure 1b). The presence of this unit makes the detailed correlation of OK1/OK2 to OK4 difficult, and thus we present the geochemical data from OK1/OK2 separately to OK4. Alignment of OK1 and OK2 is based on the top of the channel infill (located at 7 m from the base of the OK1 and at 16 m in OK2), assuming a constant sedimentation rate between both locations (Wignall & Twitchett, 2002b).

Age constraints on the Wordie Creek Formation are provided by ammonoid and conodont biostratigraphy. The first occurrence of common Early Triassic conodonts, including *Hindeodus parvus* at 8 m above the formational contact (Wignall & Twitchett, 2002b), indicate that the Permo-Triassic boundary occurs within the lower Wordie Creek Formation. This assignment is supported by the carbon isotope record from the Schuchert Dal/Fiskegrav section, in which a minimum in the carbon isotope stratigraphy is observed within the
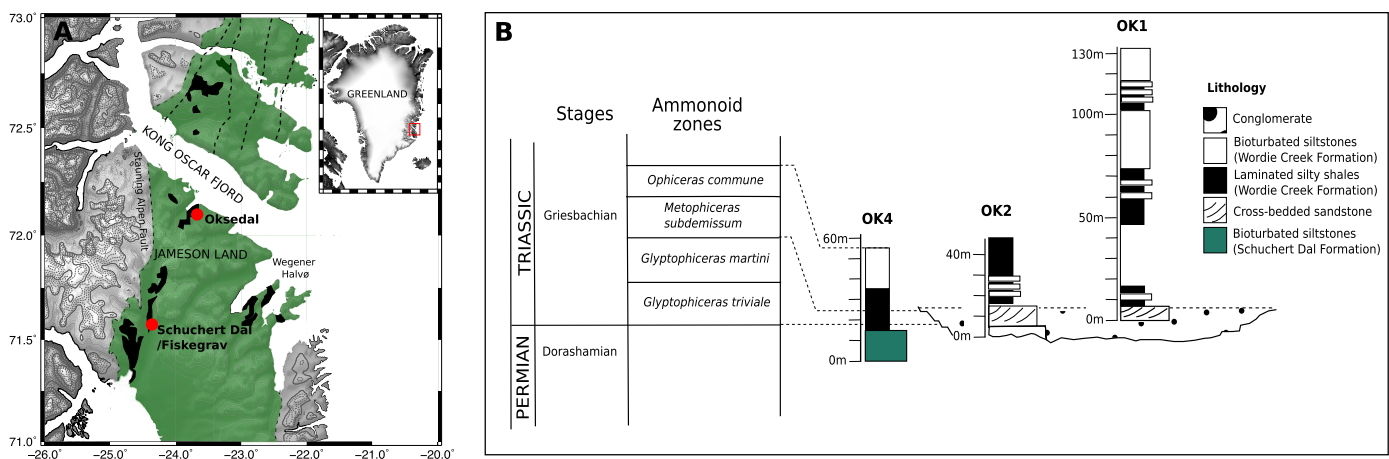

Figure 1. Location and age control of the Oksedal sections. (a) Map of the sections in East Greenland discussed here: green shaded region shows the Late Permian depositional basin, the distribution of Upper Permian sediments is shown in black. Dashed black lines show major faults in the region (modified from Stemmerik et al., 2001). (b) Age control and lithological logs of the three Oksedal sections presented in this study (modified from Wignall & Twitchett, 2002a).

lower meters of the Wordie Creek Formation (Twitchett et al., 2001). Age constraints on the remainder of the Wordie Creek Formation is provided by ammonoid biostratigraphy (Wignall & Twitchett, 2002b). The top of OK4 yields *Ophiceras commune* indicating a mid-Griesbachian age (251–250.4 Ma; Wignall & Twitchett, 2002b).

3. Analytical Methods

Shale samples were selected to be homogenous and weathered surfaces removed with a rock saw. Small chips were saved for thin section prior to sample crushing in a jaw crusher and ball-mill machine. All analysis described below was done in the Laboratory for Marine Biogeochemistry and the Godwin Laboratory in the Department of Earth Sciences at the University of Cambridge.

3.1. Sulfur Isotopes of Pyrite

Pyrite was first extracted by boiling for 1–2 h with an acidified $CrCl_2$ solution (CRS; Canfield et al., 1986; Zhabina & Volkov, 1978). Hydrogen sulfide (H_2S) produced during reduction with CRS was trapped as silver sulfide (Ag_2S), vacuum filtered and dried down for isotope analysis. Ag_2S was combusted at 1,030°C in a Flash EA coupled by continuous helium flow to a Delta V mass spectrometer. Standards NBS 127 ($\delta^{34}S = 20.3‰$ VCDT) and IAEA SO-6 ($\delta^{34}S = -34.1‰$ VCDT) were run as bracketing standards and used to correct for analytical drift in the mass spectrometer. The instrument precision is $\sigma \pm 0.24‰$, however, the method uncertainty based on replicate analyses is $\sigma \pm 0.8‰$ ($n = 26$). Weight percent pyrite was not determined during these analyses.

3.2. Sulfur Isotopes of Sulfate

Two independent methods were used to extract sulfate from the whole rock powder. The first method used the sequential digestion method (the first step of which is outlined above, section 3.1 modified from Alford et al., 2011), termed the "Thodes method" hereafter. After extracting pyrite from the rock, the residual sample was digested for 2–3 h with a strongly reducing solution of HCl, H_3PO_2, and HI (2:5:13 vol; Thode et al., 1961). This solution was added directly to the reaction vessel containing CRS solution, therefore any carbonate-associated sulfate (CAS) dissolved in the CRS solution will be liberated on addition of the Thode solution to form H_2S. The H_2S produced was trapped as Ag_2S, vacuum filtered and dried down for isotope analysis. It should be noted that this digestion will also target all remaining reducible sulfates (e.g., barite) in the rock, not only CAS. However, as CAS is likely the most abundant sulfate-bearing group, we assume that the majority of the sulfur extracted from this digestion is CAS.

A second independent method was used, following the more conventional approach for extracting CAS of Wotte et al. (2012). The sulfate in the carbonate fraction was extracted from the whole rock powder by first reacting the sample with sodium chloride solution (to leach dissolvable sulfate) and then with a 5% sodium hypochlorite/hydrogen peroxide solution (to oxidize any reduced sulfur compounds) following Wotte et al. (2012). The sample was thoroughly rinsed to remove all of the reduced sulfur compounds—the adequate number of rinses was determined by reacting aliquots of each of the sequential rinses with excess 0.1 *M* barium chloride until no precipitate was observed. The rinsed powder was then digested in a 6 *M* HCl solution at room temperature to dissolve the carbonate fraction. The effluent was then reacted with excess 0.1 *M* barium chloride solution to precipitate sulfate released from the carbonate lattice as barite, barium sulfate. The barite was rinsed three times in deionized water and dried down prior to analysis.

The sulfur isotopic composition of both the barite precipitate and the Ag_2S (from the Thodes extraction method) were analyzed via combustion at 1,030°C in a Flash EA coupled by continuous helium flow to a Delta V mass spectrometer. The weight percent sulfate was not determined during these analyses.

3.3. Carbon and Oxygen Isotopes in Carbonate and Organic Carbon

The organic carbon fraction was isolated by dissolving samples in 1 *M* HCl. The reaction was agitated for 12 h, rinsed to achieve a neutral pH and then dried. The $\delta^{13}C$ of the residual organic carbon was found by weighing 15 mg into tin capsules and combusting in an Elemental Analyzer coupled to a Thermo Finnegan MAT-253 gas source isotope-ratio mass spectrometer.

The carbonate fraction was isolated by reacting preweighed samples with 1 mL of H_2O_2 to remove organic carbon. Vials were left for 24 h with their caps loosely screwed on to allow CO_2 to escape and then placed

in an oven at 50°C to dry down. Percent organic carbon and carbonate carbon were determined gravimetrically during the above extractions.

The $\delta^{18}O_{CaCO3}$ and $\delta^{13}C_{CaCO3}$ was determined using CO_2 equilibration in a Gas Bench II coupled to a Thermo Finnegan MAT-253 gas source isotope-ratio mass spectrometer. Results are reported relative to the international Vienna Peedee Belemnite (VPDB) standard with an analytical precision of 0.08‰ for $\delta^{18}O$ and 0.06‰ for $\delta^{13}C$.

3.4. Element Concentrations in Carbonate

Weighed samples (1–2 g bulk rock) were dissolved in 50 mL of 0.1 M HNO$_3$ and then centrifuged. The supernatant solution was analyzed for Mn, Sr, and Ca concentrations on a Varian Vista ICP-OES. Initial [Ca] was determined by comparison of count intensity relative to a set of standards (whose major element chemistry broadly matched that of the carbonate solution). The [Ca] was used to determine the weight percentage CaCO$_3$. The final Mn/Ca and Sr/Ca ratios were determined at constant [Ca], to negate matrix effects. Long-term instrument precision of Mg/Ca is $\sigma \pm 0.46\%$.

3.5. Kerogen Analysis

The kerogen types from select samples from section OK4 (spanning the extinction horizon) were determined via Rock-Eval(6) pyrolysis. Approximately 5 g of sediment were ground and sieved (<63 μm). The powdered samples were treated with 36% HCl for 12 h and then 40% HF for 12 h to remove carbonates and partially remove silicates. Rock-Eval(6) pyrolysis was performed following (Słowakiewicz et al., 2015). Briefly, powdered sediments were heated from 300 to 650°C at 25°C/min in N$_2$ atmosphere and the residual carbon was then oxidised from 300 to 850°C at 20°C/min. Hydrocarbons released during the two-stage pyrolysis were measured using a flame ionization detector and CO and CO$_2$ measured using an IR cell. Rock-Eval parameters were calculated by integrating the amount of thermally vaporized free hydrocarbons (S1) and hydrocarbons released from cracking of bound OM (S2). These hydrocarbon fractions are normalized to total organic carbon (TOC) and expressed as the hydrogen index (HI) and the oxygen index (OI):

$$HI = \frac{S_2 \times 100}{TOC}$$

$$OI = \frac{S_3 \times 100}{TOC}$$

4. Results

4.1. Isotopic Changes Across the Permo-Triassic Boundary at Oksedal, Greenland

In section OK4, the $\delta^{34}S$ of pyrite displays a negative sulfur isotope excursion of 40‰ at the extinction horizon, synchronous with a negative excursion in the $\delta^{13}C$ of organic carbon of 10‰ (Figures 2a and 2b). In section OK1/OK2, which does not capture the Permo-Triassic transition, a similar coupled carbon and sulfur isotopic excursion is observed at 20–30 m; a carbon isotope excursion of -4‰ is accompanied by a -30‰ sulfur isotope excursion in the pyrite phase. Across the Early Triassic, the $\delta^{34}S_{pyr}$ increases from -25‰ to 0‰ (Figure 2b), whereas the carbon isotopic composition of organic carbon does not show a significant long-term change during the Early Triassic.

Similar to the $\delta^{34}S_{pyr}$, the sulfur isotopic composition of CAS fluctuates significantly during the Permo-Triassic boundary interval and in the Early Triassic (Figure 2b). Over the length of the Oksedal sections, the $\delta^{34}S_{CAS}$ ranges from -31 to 10‰. There is a striking correlation between the $\delta^{34}S_{CAS}$ and $\delta^{34}S_{pyr}$—in particular, across the Permo-Triassic boundary when large transient negative isotopic excursions are observed in both $\delta^{34}S_{CAS}$ and $\delta^{34}S_{pyr}$. We discuss the integrity of this $\delta^{34}S_{CAS}$ record in section 6.1.

There is no consistent isotopic excursion in the carbon or oxygen isotopic records measured on the carbonate phase (Figures 2c and 2d). The well-known -4‰ carbon isotope excursion in carbonate recorded at the Permo-Triassic boundary at other globally distributed sites (e.g., Korte & Kozur, 2010; Payne & Clapham, 2012) is not apparent in OK4, potentially suggesting diagenetic overprinting of the original signal. Additionally, the absolute oxygen isotope composition of the carbonate fraction is significantly more negative than the natural range of seawater $\delta^{18}O$.
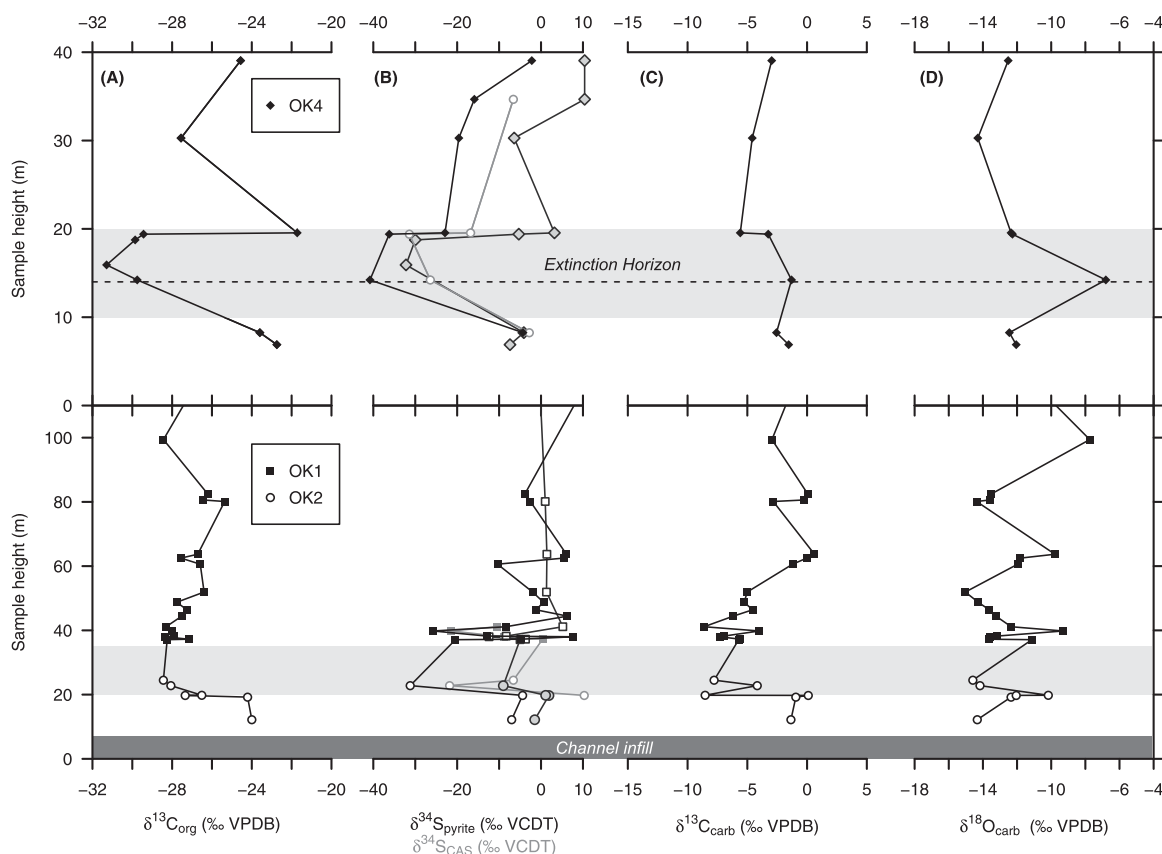
Figure 2. Carbon, sulfur, and oxygen isotopes in the Oksedal sections across the Late Permian and Early Triassic; section (top) OK4 and (bottom) OK1/OK2. (a) Carbon isotopic composition of organic carbon and (b) sulfur isotope composition of pyrite (black) and carbonate-associated sulfate (CAS; grey). Data points with blue outline indicate samples extracted by the "Thodes" method; (c) carbon isotope composition of carbonate; and (d) oxygen isotopic composition of carbonate. Grey shaded areas highlight coupled carbon and sulfur isotopic excursions. Dashed line indicated extinction horizon as defined in Wignall and Twitchett (2002a).

4.2. Weight Percent Organic Carbon and Carbonate

Weight percent organic carbon differed depending on the method used for determination; gravimetric estimates of total organic carbon (TOC) after treatment with H_2O_2 ranged between 0.02 and 0.47%, while TOC determined via pyrolysis varied between 0.03 and 1.57% (Figure 3a). We emphasize that although the absolute values are different, the trends produced via the two methods are the same, with highest TOC values observed around the extinction horizon (Figure 3a). Carbonate weight percentage was also estimate via two methods (gravimetrically after treatment with HCl and via ICP-OES); in both cases carbonate weight percentage ranged between 2 and 80% (Figure 3b), with a local minimum observed at the extinction horizon. Comparisons between the isotopic composition and the weight percent of different phases are discussed in section 6.1 to assess the potential for contamination and/or diagenetic overprinting.

4.3. Kerogen Type

The oxygen index (OI) derived from the amount of CO_2 generated during pyrolysis of the organic matter relative to TOC is used as a proxy for the amount of oxygen in the kerogen, which can be used to identify kerogen type. The OI profile shows a clear increase from the base of OK4 to the top (Figure 3d), which may reflect a change in organic matter type (source) or oxygenation conditions at the sediment-water interface. Evaluation of the hydrogen index (HI), a proxy for the amount of hydrogen in the kerogen, shows a consistent increase in values from the base of the section (7–26 mg mgCO2/g TOC), however the HI shows a slight decrease within the extinction horizon possibly indicating a change in either the supply or type of organic matter (Figure 3c). In comparison to the possible HI range of organic matter, the sediments from OK4 section have relatively low HI values (<50 mg CO_2/g TOC), which reflects type IV kerogen. There is no change in kerogen type across the extinction horizon.
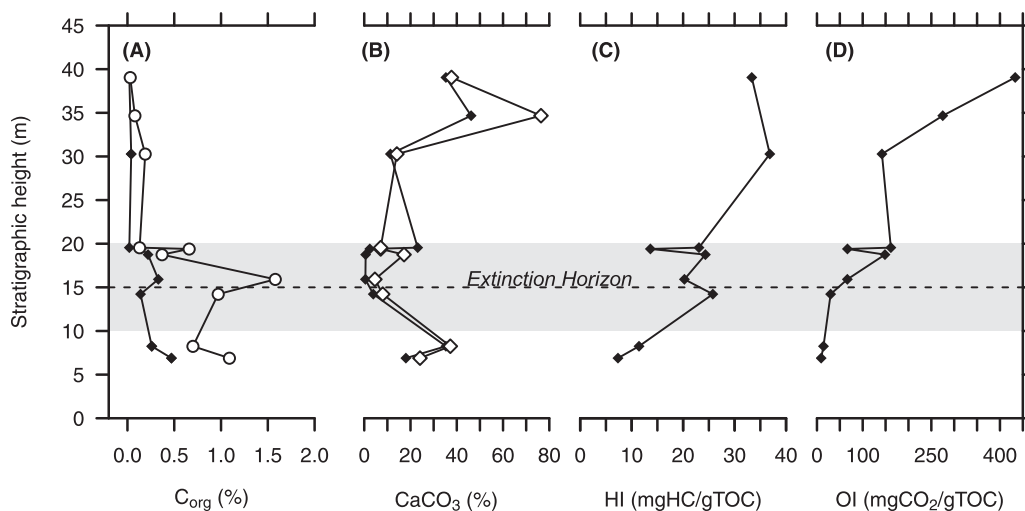
Figure 3. Weight percentage organic carbon and carbonate, hydrogen, and oxygen indices in section OK4. (a) Weight percentage organic carbon determined gravimetrically after treatment with H_2O_2 (black symbols) and via pyrolysis (white symbols); (b) weight percentage carbonate determined gravimetrically after treatment with HCl (black symbols) and via ICP-OES (white symbols); (c) hydrogen index of kerogen fraction; and (d) oxygen index of kerogen fraction.

5. Discussion

In the following discussion, we review the evidence for secondary alteration of the different geochemical phases measured (section 6.1), and conclude that in these sections, the isotopic composition of the carbonate phase has been altered whereas organic carbon and pyrite phases appear to be primary. We then discuss the nature and timing of the chemical alteration of the carbonate phase (section 6.2). The second half of this discussion covers the better preserved organic carbon and pyrite isotopic records across the Permo-Triassic boundary and the potential environmental implications of these records (section 6.3).

5.1. Integrity of Isotopic Compositions

In this section, we review the fidelity of the different geochemical records measured and the evidence for diagenetic alteration of the isotopic compositions of each phase.

5.1.1. Contamination During Sample Preparation

During the separation of different carbon and sulfur mineral phases, it is possible that contaminant phases were only partially digested and could therefore influence the carbon or sulfur isotope composition of the
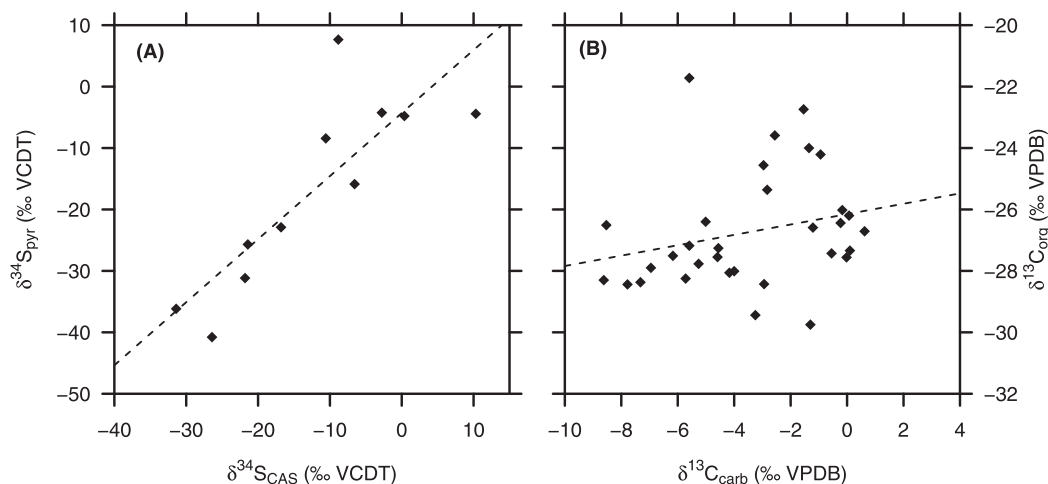

Figure 4. Correlation between the isotopic composition of different sulfur-bearing and carbon-bearing minerals in the Oksedal section. (a) Crossplot of pyrite and carbonate-associated sulfate sulfur isotopes (extracted following Wotte et al., 2012). (b) Crossplot of organic carbon and carbonate carbon isotopes.
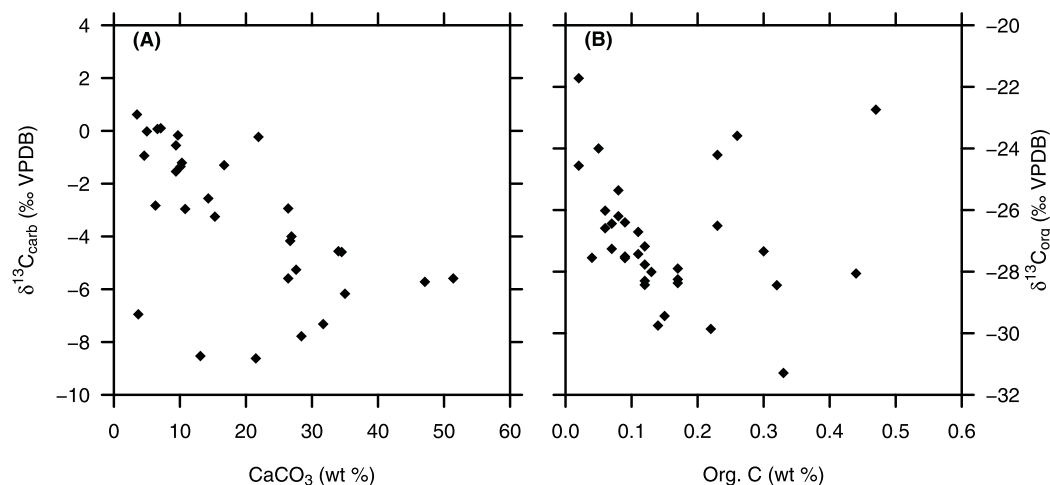
Figure 5. Isotopic signatures of (a) carbonate and (b) organic carbon, plotted against weight percentage abundance of each mineral phase for the Oksedal sections.

target phase. Comparison of the $\delta^{34}S$ of sulfur-bearing mineral phases (CAS and pyrite; Figure 4a) reveals a strong correlation ($R^2 = 0.7$). By contrast, a weaker correlation ($R^2 = 0.2$) is observed between organic carbon and carbonate $\delta^{13}C$ (Figure 4b).

In sequential extractions such as these, a strong positive correlation between the $\delta^{34}S$ of sulfur-bearing mineral phases may be observed if pyrite (oxidized during extraction) contaminated the sulfate fraction. However, it should be noted that sulfate was extracted from the whole rock using two independent methods which yielded similar isotopic results (Figure 2b). Given that the Wotte et al. (2012) type extraction involved thorough rinsing after the sulfide extraction, we would expect that the contamination of pyrite (oxidized during extraction) would be negligible. By contrast, the Thode extraction did not involve rinsing in between the sulfide and sulfate extractions, therefore contamination might be more of an issue here. It is therefore difficult to explain the similarity of the $\delta^{34}S_{SO4}$ records from the two extractions in the context of contamination during extraction. Instead, we argue that secondary alteration is a more likely explanation for the strong positive correlation between the $\delta^{34}S_{SO4}$ and the $\delta^{34}S_{pyr}$: if, for example, isotopically negative pyrite is oxidized into sedimentary porewaters, then reprecipitated as sedimentary sulfate, this has the potential to overprint the primary sulfate signal (e.g., Rennie & Turchyn, 2014).

Evidence of a contaminated isotopic signal may also be evaluated by crossplotting the weight percentage of specific mineral phases against their isotopic composition. If sample contamination has occurred, one might expect that samples containing a low concentration of a specific target phase might be more strongly affected by contamination. There is no significant correlation between weight percent carbonate and its isotopic composition ($R^2 = 0.001$; Figure 5a), suggesting that any contamination has not had a significant effect on the isotopic composition of these samples. A similar result is found for organic carbon ($R^2 = 0.03$; Figure 5b). The same approach cannot be used for assessing potential contamination in the sulfur phases, as weight percentage sulfate and pyrite were not determined.

5.1.2. Alteration of the Carbonate Phase

Geochemical evidence can be used to assess the hypothesis that the carbonate phases have been altered since deposition, either through burial diagenesis or through interaction with later-stage fluids. We note several lines of evidence that suggest that the isotopic signatures in the carbonate phase are not primary. The first line of evidence is that the $\delta^{18}O_{carb}$ is significantly outside of the range of carbonate precipitated from seawater $\delta^{18}O$, suggesting some secondary process has lowered the $\delta^{18}O_{carb}$. The second line of evidence suggesting alteration of the carbonate minerals is derived through comparison of Mn/Sr ratios with the $\delta^{13}C$ of carbonate and organic carbon. Strontium is often released from carbonate minerals during burial while manganese, which can be high in porewater due to reductive mobilization, is similarly enriched in the recrystallized carbonate phase; thus a high Mn/Sr ratio is often interpreted to reflect a greater degree of burial diagenesis (Jacobsen & Kaufman, 1999). As discussed in section 6.1.1, burial diagenesis often results in lower carbonate $\delta^{13}C$; oxidation of isotopically lower organic carbon and the subsequent
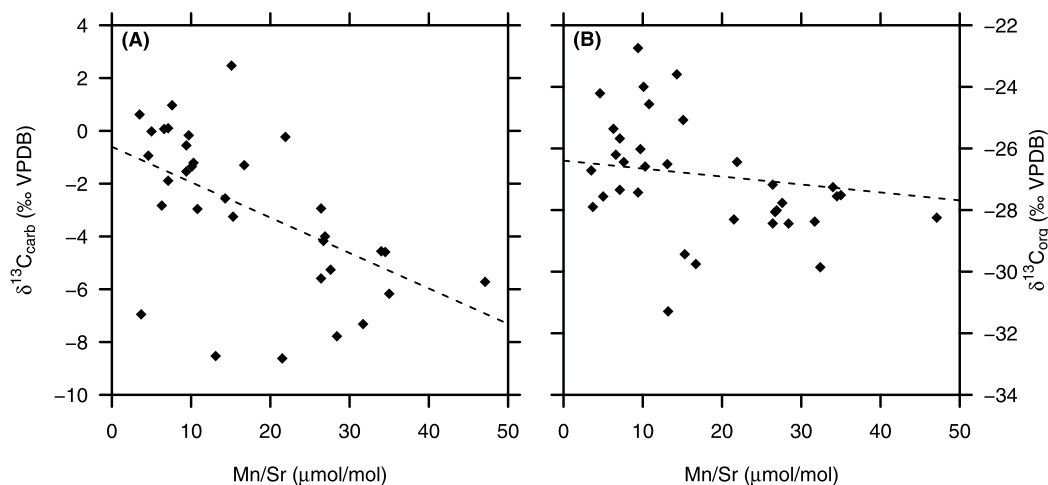
Figure 6. Assessing the influence of diagenetic alteration on the isotopic signatures of carbonate. The Mn/Sr ratio was measured in the carbonate phase and is used here as a proxy for the extent of diagenetic alteration, see text.

reprecipitation of calcium carbonate would produce more negative carbonate δ^{13}C. The negative correlation between Mn/Sr and $\delta^{13}C_{carb}$ ($R^2 = 0.2$; Figure 6a) supports diagenetic replacement in some of the samples. In contrast, the correlation between Mn/Sr and $\delta^{13}C_{org}$ is small ($R^2 = 0.02$; Figure 6b), suggesting little effect of burial diagenesis on the δ^{13}C of organic carbon. The final line of evidence comes from the comparison of the record of $\delta^{34}S_{CAS}$ with $\delta^{34}S_{pyr}$ (Figure 4a); the strong correlation between the two records and the highly negative $\delta^{34}S_{CAS}$ suggests that the sulfate in the carbonate phase has been influenced by the presence of an isotopically light phase of sulfur, most likely derived from pyrite through oxidation, during alteration of the carbonate phase. Although this could arguably be an artefact of contamination during the laboratory extraction, taken with the negative $\delta^{18}O_{carb}$ and correlations with Mn/Sr, it is equally possible that pyrite oxidation occurred during alteration when the oxygen and carbon isotopes were reset, and that this sulfate was incorporated into the CAS, causing the correlation in $\delta^{34}S_{CAS}$ and $\delta^{34}S_{pyr}$. This would suggest that it is the colocal pyrite that is oxidized and, during subsequently incorporated into sulfate during later-stage alteration, impacting the $\delta^{34}S_{CAS}$, rather than a separate source that is isotopically homogenous and has reset the local CAS at one time. Pyrite oxidation lowers pH and may be a driver for local carbonate dissolution and then oxidation and carbonate reprecipitation.

In summary, the isotopic composition associated with the carbonate mineral phase ($\delta^{13}C_{carb}$, $\delta^{18}O_{carb}$, and $\delta^{34}S_{CAS}$) appears to have been altered either during burial diagenesis or through interaction with a secondary fluid. By contrast, we argue that the organic carbon δ^{13}C and pyrite δ^{34}S have retained their primary isotopic composition.

5.2. Timing of Carbonate Alteration

Is there anything to be learned from the carbon and isotope composition of carbonate minerals that clearly have been recrystallized? First, we discuss the potential candidates for a secondary fluid (that would have been involved with the alteration of the carbonate mineral phases), and then we use a water-rock interaction model to explore the timing of carbonate alteration in these samples.

Alteration of carbonate rocks through isotopic equilibration of the primary carbonate with fluids of differing oxygen isotope composition is known to impact the δ^{18}O of the carbonate. The partitioning of oxygen isotopes between fluid and carbonate is highly temperature dependent and therefore reequilibration of carbonates at depth (and therefore at higher temperatures) will result in isotopically lower carbonate δ^{18}O (Matter et al., 1975; Schrag et al., 1995). The carbonate δ^{18}O in the Oksedal section have an average of $-12.5 \pm 2.3‰$. Given the lack of polar icecaps during the latest Permian and Early Triassic (Ziegler, 1990), deep ocean water δ^{18}O should have been approximately 0‰. The offset of 12.5‰ implies that carbonate minerals isotopically equilibrated with fluids at a temperature of approximately 50°C (Kim & O'Neil, 1997). There are two scenarios in which the temperature during reequilibration may become elevated above the initial temperature in which the primary carbonate was formed: (i) the influence of intrusive igneous bodies

and (ii) burial and geothermal heating. Evidence of Tertiary volcanism from the North Atlantic Igneous Province (circa 60 Ma) can be clearly seen in many regions in East Greenland. However, in the Oksedal sections, the color and exceptional preservation of palynomorphs (Looy et al., 2001) and the very low color alteration index of Wordie Creek Formation conodonts indicates unequivocally that the section is immature (Grotheer et al., 2016). We therefore argue that high temperature alteration is not responsible for the isotopically lower $\delta^{18}O$ in carbonate measured here.

Instead, we suggest that the low $\delta^{18}O$ reflects interaction with a fluid depleted in ^{18}O relative to seawater, and that meteoric water is a likely candidate for this fluid. The pattern of alteration of marine sediments by meteoric fluids has been described by Lohmann (1987) as following an inverted "J" pattern in carbon and oxygen isotope space. The original carbonate mineral $\delta^{18}O$ will tend toward more negative values following interaction with meteoric water. At the same time, oxidized organic matter in that meteoric water simultaneously will lower the $\delta^{13}C$. Due to the larger concentration of carbon in carbonate sediment compared to dissolved carbon in the interacting fluid, altering the $\delta^{13}C$ of the carbonate minerals takes significantly more water-rock interaction than shifting the carbonate mineral $\delta^{18}O$. We model this alteration following Jacobsen and Kaufman (1999; see supporting information for model details).

Geochemical records from across the Permo-Triassic transition show evidence of significant changes in unaltered carbonate $\delta^{13}C$ and $\delta^{18}O$ (Korte & Kozur, 2010; Sun et al., 2013), suggesting large changes in mean ocean $\delta^{13}C_{DIC}$ and global temperatures. We therefore explore the sensitivity of the model to different initial isotopic compositions of the carbonate minerals that were originally deposited (Figure 7). The Oksedal carbonate $\delta^{13}C$-$\delta^{18}O$ data plot outside the range of possible initial carbonate $\delta^{13}C$-$\delta^{18}O$ compositions, suggesting that significant water-rock interaction has occurred. The Oksedal carbonate rocks primarily reflect the isotopic composition of the interacting fluid rather than the initial carbonate.

We can therefore use the Oksedal carbonates to constrain the isotopic composition of the interacting fluid. In this model, we use an initial carbonate isotopic composition of $\delta^{18}O = 0\%_o$ and $\delta^{13}C = 4\%_o$ (Jacobsen & Kaufman, 1999). Our model suggests that the $\delta^{13}C$ of the secondary fluid was less than $-10\%_o$. Fitting the
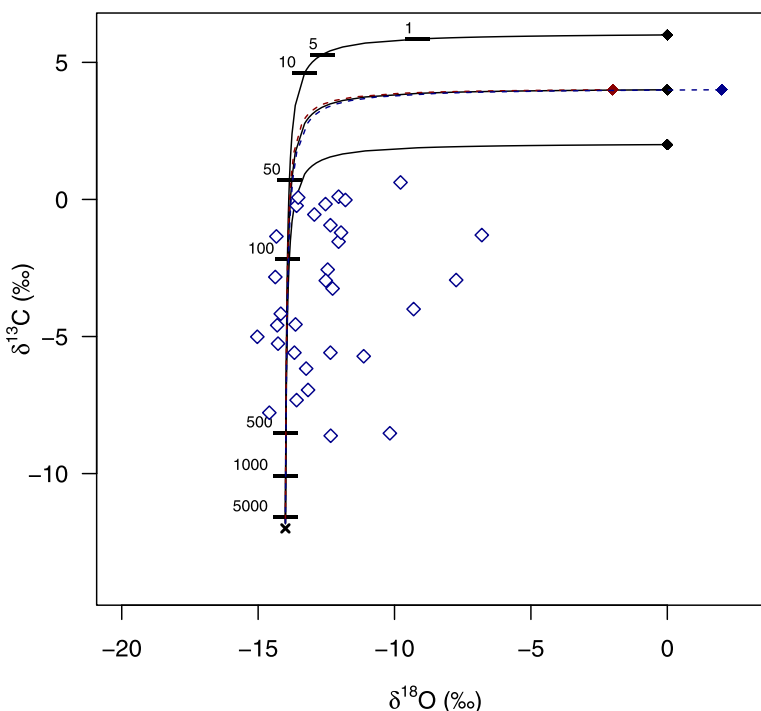

Figure 7. Sensitivity of final rock isotopic composition to varying degrees of water-fluid interaction given different initial rock isotopic compositions. Closed diamonds show different initial composition scenarios. Open diamonds shown Oksedal carbonate isotopic compositions. The numbers show the degree of water-rock interaction (η).

majority of the $\delta^{18}O$ data, we suggest than the $\delta^{18}O$ composition of the interacting fluid was between -12 and $-15‰$ (Figure 7).

Oxygen isotope fractionation during evaporation of seawater results in ^{16}O-rich meteoric water. However, the degree of oxygen isotope fractionation is known to depend on sea surface temperature, and therefore varies strongly with latitude (Fricke & O'Neil, 1999). Using an initial $\delta^{18}O$ of meteoric water based on Fricke and O'Neil (1999), the model of water-rock interaction was used to compare the isotopic mixing curves at various latitudes with the isotopic composition of the carbonate in the three studied sections (Figure 8). Given our constraints on the isotopic composition of the fluid, we suggest that the meteoric fluid likely was derived from a latitude of 50°N to 55°N. This latitude is significantly northward of palaeo-latitude estimated for Greenland at the Permo-Triassic transition (roughly 40°N; Twitchett et al., 2001; Wignall & Twitchett, 2002a), and therefore suggests that the main phase of alteration of the carbonate phase occurred substantially (millions of years) after the initial deposition.

Interestingly, the isotopic composition of the interacting fluid is not consistent with meteoric water from 70°N (the latitude of Greenland during the formation of the North Atlantic Igneous Province). The North Atlantic Igneous Province ($\sim$60 Ma) has been invoked to explain other geochemical heterogeneity in the region (Surlyk et al., 1986). While the Oksedal $\delta^{18}O$-$\delta^{13}C$ are latitudinally inconsistent with a meteoric water source from 70°N, we emphasize that strong local variations in the $\delta^{18}O$ of meteoric water are possible, which may result in significant deviations in the $\delta^{18}O$ of meteoric water from that predicted from latitude (Fricke & O'Neil, 1999). Furthermore, as the Permo-Triassic transition was free of polar icecaps, the mean seawater $\delta^{18}O$ would be approximately $1‰$ lower than it is today, and the surface patterns of $\delta^{18}O$ might be markedly different. We therefore emphasize the uncertainty in our estimates of the palaeo-latitude of recrystallization.

While we acknowledge uncertainties in the isotopic composition of the rock and the fluid, our water-rock interaction modeling exercise supports our hypothesis that the carbonate in the Oksedal section has been significantly altered. Based on the assumed initial isotopic values of the rock ($\delta^{13}C = 5‰$, $\delta^{18}O = 0‰$) and the water ($\delta^{13}C = -12‰$, $\delta^{18}O$ dependent on latitude), the model suggests that the weight ratio of
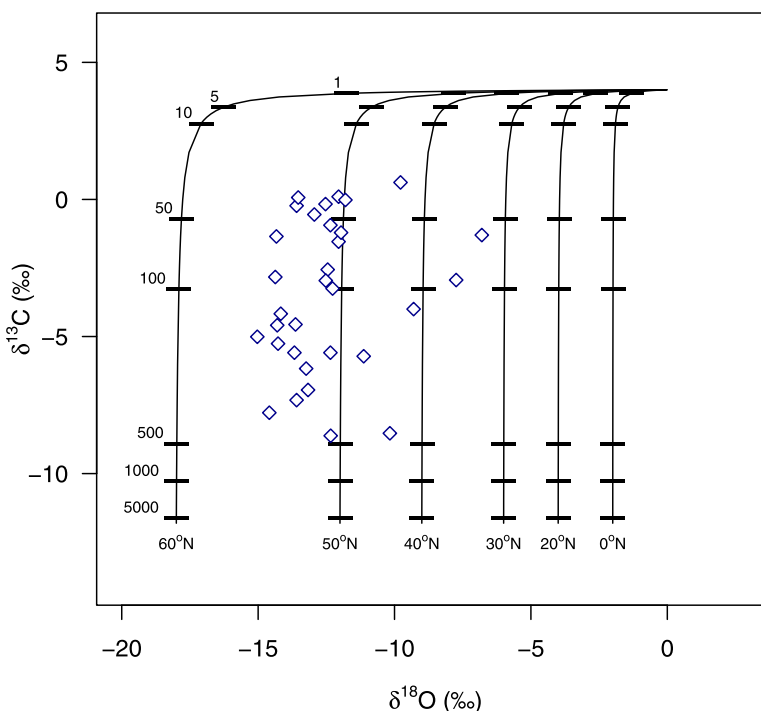

Figure 8. Water-rock interaction model used to assess the timing of carbonate recrystallization in Oksedal using the oxygen isotope composition of meteoric water as a function of latitude and a range of water-rock ratios (black values) during recrystallization. These data suggest that the carbonate was recrystallized when Greenland was around 50°N.

meteoric water to rock ranges between 20 and 500. The corollary of this water-rock interaction modeling is that geochemical data from Oksedal carbonate minerals can be used as a primary archive only when the concentration of the element within the rock vastly exceeds that of the meteoric water interacting with it.

5.3. The Perturbation at the Boundary

Given that the carbonate records in the Oksedal section are strongly affected by late-stage alteration, we now turn to the organic carbon and pyrite records, which we argue are better preserved (section 6.1). We will discuss interpretations of these geochemical archives and their implications for environmental changes within the Jameson Land Basin across the Permo-Triassic transition.

The Oksedal sections reveal a 40‰ negative excursion in $\delta^{34}S_{pyr}$ coupled with a 10‰ negative excursion in $\delta^{13}C_{org}$ immediately after the extinction horizon. Coupled negative organic carbon and pyrite-sulfur isotope excursions have been observed in other Permo-Triassic sections globally (Algeo et al., 2008; Luo et al., 2010), with the addition of euxinic waters from deeper within the basin invoked to explain the covariation. Organic matter oxidation and sulfur isotope fractionation during sulfate reduction results in a low $\delta^{13}C$ and low $\delta^{34}S_{H2S}$, and elevated $\delta^{34}S_{SO4}$ in deep euxinic water masses. If upwelled, euxinic, low-$\delta^{13}C$ water promotes photosynthesis then its "light" signal will be captured in $\delta^{13}C_{org}$, while upwelling of euxinic waters followed by pyrite precipitation generates a negative shift in $\delta^{34}S_{pyr}$ if the upwelled sulfide is directly captured as syngenetic pyrite (Algeo et al., 2008).

Euxinic conditions in the Jameson Land Basin have been suggested on the basis of pyrite framboid studies (Bond & Wignall, 2010; Nielsen et al., 2010; Wignall & Twitchett, 2002a); however, we suggest that several new lines of evidence are inconsistent with the idea of basin-wide euxinia. First, in order to produce the observed isotopic excursion of −40‰ in the bulk pyrite signal (as observed in the Oksedal sections), mass balance dictates that almost ten times as much syngenetic pyrite (with an average $\delta^{34}S_{pyr} = -45‰$; Algeo et al., 2008) would need to be buried relative to authigenic pyrite (with an average $\delta^{34}S_{pyr} = 0‰$; Algeo et al., 2008) during the intervals of hypothesized euxinia. This ratio is significantly larger than the ratios observed in other Permo-Triassic sections (which range between 1:1 and 4:1; Algeo et al., 2008). This suggests either than the Jameson Land Basin became intensely euxinic (Bond & Wignall, 2010) or that other processes in addition to the burial of isotopically negative $\delta^{34}S$ syngenetic pyrite produced the signal seen in our record. Second, our hydrocarbon analysis of the Oksedal section suggests that all kerogen is type IV, which is thought to reflect reworked terrestrially derived organic carbon. The negative $\delta^{13}C_{org}$ excursion in the Jameson Land Basin therefore is not reflective of changes in marine dissolved inorganic carbon $\delta^{13}C$ and provides no direct evidence for upwelled euxinic water. Third, marked differences between the Oksedal $\delta^{34}S_{pyr}$ record and other previously published records from the Fiskegrav section (~100 km south of Oksedal; Fenton et al., 2007; Mettam et al., 2017; Nielsen et al., 2010; Stemmerik et al., 2001; Twitchett et al., 2001) argues against intense basin-wide euxinia. Across the Late Permian and Early Triassic, the Jameson Land Basin was a north-facing open embayment at the southern end of the East Greenland rift system (Surlyk et al., 1986; Wignall & Twitchett, 2002b). The Oksedal sections were further from the basin margin and likely in deeper water than the Fiskegrav site—interpreted to have a maximum depth of 100 m (Mettam et al., 2017). Across the Permo-Triassic transition, both Oksedal and Fiskegrav witness a 10‰ negative excursion in $\delta^{13}C_{org}$ (Figure 9b); however, the $\delta^{34}S_{pyr}$ is markedly different between the two locations (Figure 9a). In Fiskegrav, there is variability in $\delta^{34}S_{pyr}$ before the extinction horizon, but no apparent excursion at the horizon, whereas, in the Oksedal sections, a transient −40‰ excursion is observed in $\delta^{34}S_{pyr}$ across the extinction horizon. If the negative sulfur isotope excursion in the Oksedal sections was attributable to the increased burial of isotopically more negative syngenetic pyrite due basin-wide euxinia, we would predict that the shallower Fiskegrav section would also show a negative sulfur isotopic excursion (albeit of a smaller magnitude, if euxinia was less prevalent in shallower environments). This is not the case. The final line of evidence against basin-wide euxinia comes from a recent study of iron speciation in the Fiskgrav section (Mettam et al., 2017). This shows that although anoxic conditions were likely prevalent, long-term euxinia was not achieved.

Regional heterogeneity in sulfur isotopic compositions following the Permo-Triassic mass extinction is not unique to East Greenland, indeed similar pyrite-sulfur isotopic disparities have been observed in other sections globally (Payne & Clapham, 2012). In the case of the Jameson Land Basin, we acknowledge that dating uncertainties at the two locations mean we cannot be certain that we are comparing samples from the
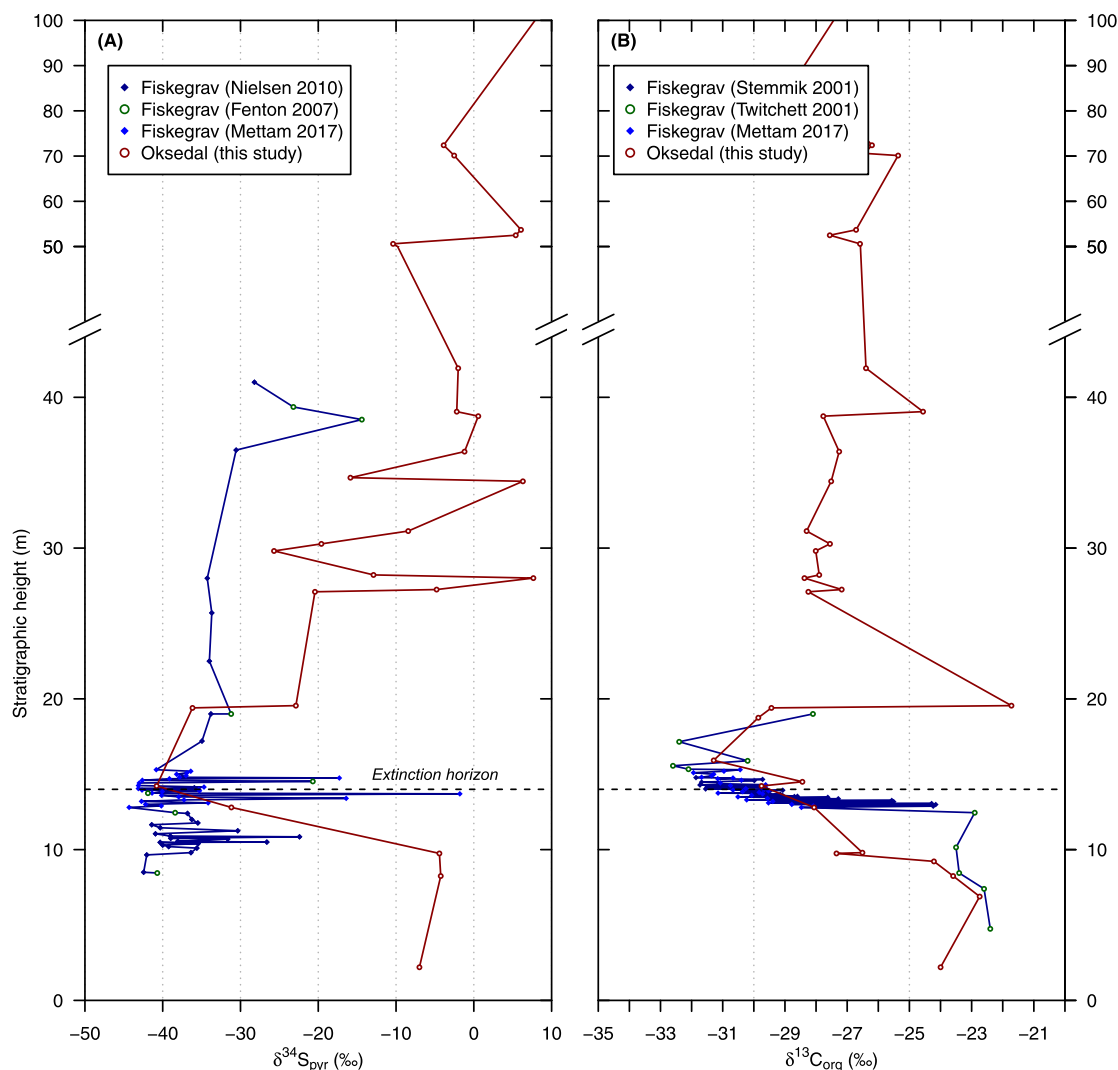
Figure 9. Compilation of (a) $\delta^{34}S_{pyr}$ and (b) $\delta^{13}C_{org}$ spanning the Permo-Triassic in East Greenland. Several different records from Fiskegrav are shown, with references to the original publications shown in the legend. The Fiskegrav and Oksedal sections were aligned using the base of the Wordie Creek Formation as a tie-point and assuming a constant regional sedimentation rate.

same stratigraphic horizon, however for the purpose of this discussion we will assume that the previously determined stratigraphic analysis is correct (Wignall & Twitchett, 2002b) and the excursions in the carbon isotope composition of organic matter can be correlated. This discussion then centers around how two sections 100 km apart could have a similar change in $\delta^{13}C_{org}$ but a markedly different change in $\delta^{34}S_{pyr}$.

The carbon isotope composition of organic carbon in any given sediment largely reflects the type of the organic carbon in that particular sediment. The kerogen in the Oksedal sections is dominantly type IV, and there is no apparent change in the kerogen type across the extinction horizon. As type IV kerogen is interpreted to reflect reworked organic matter derived from terrestrial sources, we suggest that the negative $\delta^{13}C_{org}$ excursion in the Jameson Land Basin reflects (i) a global change in $\delta^{13}C$, which extended to the atmosphere as well as the ocean (Berner, 2002), (ii) a change in the flux of organic carbon derived from terrestrial sources, or (iii) a change in the preservation of organic carbon across the Permo-Triassic transition. Higher TOC across the Permo-Triassic transition (Figure 3a), which is synchronous with the negative $\delta^{13}C_{org}$ excursion, may indicate better preservation of organic carbon or an elevated flux of terrestrial-derived organic carbon to the basin during this interval. We emphasize that, as there appears to be no evidence of marine-derived organic carbon remaining in these sections, the $-4‰$ isotopic excursion $\delta^{13}C$ excursion observed in many marine sections at the Permo-Triassic boundary (Korte & Kozur, 2010) likely extended

beyond the marine realm. Irrespective of the source of the $\delta^{13}C_{org}$ excursion, the similar magnitude and timing (relative to the extinction horizon) of the $\delta^{13}C_{org}$ excursion at both sites supports the idea that basin-wide shifts in $\delta^{13}C_{org}$ occurred at the Permo-Triassic transition.

The $\delta^{34}S_{pyr}$, unlike the $\delta^{13}C_{org}$, does not change uniformly across the Jameson Land Basin, suggesting it largely reflects local diagenetic processes within the sediment column and not changes in the sulfur isotope composition of the overlying water change. Pyrite is formed from sulfide produced during microbial sulfate reduction, and microbial sulfate reduction partitions sulfur isotopes between 0 and 70‰ (Canfield et al., 2010). The magnitude of this sulfur isotope fractionation is largely a function of the rate of microbial sulfate reduction, which itself varies with temperature, source of carbon, and amount of sulfate (Canfield et al., 2010; Chambers & Trudinger, 1979; Johnston et al., 2005, 2007). Pyrite-sulfur isotopic composition therefore reflects changes in any of these local environmental conditions in the sediment. Furthermore, $\delta^{34}S_{pyr}$ can also change as a function of the depth of pyrite formation in the sediment column; pyrite that forms shallower, in more open connection to the overlying water (and the source of sulfate) has a lower overall $\delta^{34}S_{pyr}$, while the pyrite that forms deeper, where the sulfate $\delta^{34}S$ is more evolved will have a higher overall $\delta^{34}S_{pyr}$ (Aller et al., 2010; Fike et al., 2015).

Before the Permo-Triassic extinction horizon, the $\delta^{34}S_{pyr}$ of the Fiskegrav section is around 30‰ more negative than the $\delta^{34}S_{pyr}$ of Oksedal. This could indicate different dynamics for microbial sulfate reduction and pyrite formation in the deep site relative to the shallower water location. This difference can be explained several ways. First, the depth of microbial sulphate reduction may have been deeper in the sediment column in the Oksdeal location, resulting in higher $\delta^{34}S_{pyr}$. A second possibility is that sediment reworking, either biologically or through other physically induced mechanisms, impacts the overall $\delta^{34}S_{pyr}$ that is preserved (Fike et al., 2015). In this hypothesis, sediment reworking can partially reoxidize precipitated phases, subsequent rereduction of sulphate will generate isotopically very low $\delta^{34}S_{pyr}$. In this case, prior to the Permo-Triassic boundary, the Fiskegrav section reflects enhanced bioturbation and the Oksedal section reflects less sediment reworking and microbial sulfate reduction operating under more closed system conditions.

If we stretch this idea further, we could hypothesize that across the Permo-Triassic boundary, the decrease in $\delta^{34}S_{pyr}$ at Oksedal could be the result of microbial sulfate reduction moving shallower in the sediment column in response to a change in the supply of organic carbon. An alternative possibility is that the physical biological reworking of the sediments becomes stronger at depth, generating enhanced reoxidation of sulfide phases and transient preservation of isotopically lower pyrite. By contrast, the lack of change in the Fiskegrav section $\delta^{34}S_{pyr}$ across the Permo-Triassic boundary suggests that microbial sulfate reduction continued to operate under open system conditions, although we note the existence of several samples with markedly higher $\delta^{34}S_{pyr}$ (potentially suggesting short-lived intervals of closed system microbial sulfate reduction).

6. Conclusion

We presented sulfur and carbon isotopic records from the expanded Permo-Triassic boundary Oksedal sections in East Greenland. These records suggest a 40‰ negative sulfur isotope excursion in pyrite and a 10‰ negative carbon isotope excursion in organic carbon across the Permo-Triassic boundary. In contrast, the isotopic records of oxygen, carbon and CAS appear to have been altered by postdepositional recrystallization.

A simple water-rock interaction model was used to determine the extent and nature of carbonate recrystallization in the Oksedal sections. We suggest that the carbon and oxygen isotopic values are most consistent with significant (20–500 water to rock ratio) interaction of the original carbonate with meteoric water significantly after initial deposition.

Comparison of $\delta^{13}C_{org}$ and $\delta^{34}S_{pyr}$ records from the Oksedal sections (which we argue were unaffected by late-stage alteration) with a proximal site in East Greenland shows marked regional variability in $\delta^{34}S_{pyr}$ across the Permo-Triassic transition despite similar changes in $\delta^{13}C_{org}$. Given this heterogeneity in $\delta^{34}S_{pyr}$ and our evidence that the organic carbon in the Oksedal sections was dominantly type IV—reflecting reworked terrestrial organic carbon, we suggest that long-term, basin-wide euxinia cannot explain the

trends in $\delta^{34}S_{pyr}$. Instead, we propose that variations in the position of sulfate reduction within the sediment column in response to a change in the flux or preservation of organic carbon into the Jameson Land Basin may affect the fractionation of sulfur. This process can lead to regional heterogeneity in records of $\delta^{34}S_{pyr}$. Testing this hypothesis would require unaltered isotopic records of sulfate, which are not available from these locations.

References

Alford, S. E., Alt, J. C., & Shanks, W. C. (2011). Sulfur geochemistry and microbial sulfate reduction during low-temperature alteration of uplifted lower oceanic crust: Insights from ODP Hole 735B. *Chemical Geology*, *286*(3), 185–195. https://doi.org/10.1016/j.chemgeo.2011.05.005

Algeo, T., Shen, Y., Zhang, T., Lyons, T., Bates, S., Rowe, H., & Nguyen, T. K. T. (2008). Association of ^{34}S-depleted pyrite layers with negative carbonate δ^{13}C excursions at the Permian-Triassic boundary: Evidence for upwelling of sulfidic deep-ocean water masses. *Geochemistry, Geophysics, Geosystems*, *9*,Q04025. https://doi.org/10.1029/2007GC001823

Aller, R. C., Madrid, V., Chistoserdov, A., Aller, J. Y., & Heilbrun, C. (2010). Unsteady diagenetic processes and sulfur biogeochemistry in tropical deltaic muds: Implications for oceanic isotope cycles and the sedimentary record. *Geochimica et Cosmochimica Acta*, *74*(16), 4671–4692. https://doi.org/10.1016/j.gca.2010.05.008

Berner, R. A. (2002). Examination of hypotheses for the Permo–Triassic boundary extinction by carbon cycle modeling. *Proceedings of the National Academy of Sciences of the United States of America*, *99*(7), 4172–4177. https://doi.org/10.1073/pnas.032095199

Bond, D. P. G., & Wignall, P. B. (2010). Pyrite framboid study of marine Permian-Triassic boundary sections: A complex anoxic event and its relationship to contemporaneous mass extinction. *Bulletin of the Geological Society of America*, *122*(7–8), 1265–1279. https://doi.org/10.1130/B30042.1

Canfield, D. E., Farquhar, J., & Zerkle, A. L. (2010). High isotope fractionations during sulfate reduction in a low-sulfate euxinic ocean analog. *Geology*, *38*(5), 415–418. https://doi.org/10.1130/G30723.1

Canfield, D. E., Raiswell, R., Westrich, J. T., Reaves, C. M., & Berner, R. A. (1986). The use of chromium reduction in the analysis of reduced inorganic sulfur in sediments and shales. *Chemical Geology*, *54*(1–2), 149–155.

Chambers, L. A., & Trudinger, P. A. (1979). Microbiological fractionation of stable sulfur isotopes: A review and critique. *Geomicrobiology Journal*, *1*(3), 249–293. https://doi.org/10.1080/01490457909377735

Fenton, S., Grice, K., Twitchett, R. J., Böttcher, M. E., Looy, C. V., & Nabbefeld, B. (2007). Changes in biomarker abundances and sulfur isotopes of pyrite across the Permian–Triassic (P/Tr) Schuchert Dal section (East Greenland). *Earth and Planetary Science Letters*, *262*(1), 230–239.

Fike, D. A., Bradley, A. S., & Rose, C. V. (2015). Rethinking the ancient sulfur cycle. *Annual Review of Earth and Planetary Sciences*, *43*(1), 593–622. https://doi.org/10.1146/annurev-earth-060313-054802

Fricke, H. C., & O'Neil, J. R. (1999). The correlation between ^{18}O/^{16}O ratios of meteoric water and surface temperature: Its use in investigating terrestrial climate change over geologic time. *Earth and Planetary Science Letters*, *170*(3), 181–196.

Grotheer, H., Le Métayer, P., Piggott, M. J., Lindeboom, E. J., Holman, A. I., Twitchett, R. J., & Grice, K. (2016). Occurrence and significance of phytanyl arenes across the Permian-Triassic boundary interval. *Organic Geochemistry*, *104*, 42–52.

Jacobsen, S. B., & Kaufman, A. J. (1999). The Sr, C and O isotopic evolution of Neoproterozoic seawater. *Chemical Geology*, *161*(1–3), 37–57.

Johnston, D. T., Farquhar, J., & Canfield, D. E. (2007). Sulfur isotope insights into microbial sulfate reduction: When microbes meet models. *Geochimica et Cosmochimica Acta*, *71*(16), 3929–3947. https://doi.org/10.1016/j.gca.2007.05.008

Johnston, D. T., Farquhar, J., Wing, B. A., Kaufman, A. J., Canfield, D. E., & Habicht, K. S. (2005). Multiple sulfur isotope fractionations in biological systems: A case study with sulfate reducers and sulfur disproportionators. *American Journal of Science*, *305*(6–8 Spec. Iss.), 645–660. https://doi.org/10.2475/ajs.305.6-8.645

Kim, S.-T., & O'Neil, J. R. (1997). Equilibrium and nonequilibrium oxygen isotope effects in synthetic carbonates. *Geochimica et Cosmochimica Acta*, *61*(16), 3461–3475.

Korte, C., & Kozur, H. W. (2010). Carbon-isotope stratigraphy across the Permian–Triassic boundary: A review. *Journal of Asian Earth Sciences*, *39*(4), 215–235.

Lohmann, K. C. (1988). Geochemical patterns of meteoric diagenetic systems and their application to studies of paleokarst (pp. 58–80). In N. P. James, & P. W. Choquette (Eds.), Paleokarst. New York, NY: Springer.

Looy, C. V., Twitchett, R. J., Dilcher, D. L., Van Konijnenburg-Van Cittert, J. H., & Visscher, H. (2001). Life in the end-Permian dead zone. *Proceedings of the National Academy of Sciences of the United States of America*, *98*(14), 7879–7883.

Luo, G., Kump, L. R., Wang, Y., Tong, J., Arthur, M. A., Yang, H., . . . Xie, S. (2010). Isotopic evidence for an anomalously low oceanic sulfate concentration following end-Permian mass extinction. *Earth and Planetary Science Letters*, *300*(1–2), 101–111.

Matter, A., Douglas, R. G., & Perch-Nielson, K. (1975). Fossil preservation, biochemistry, and diagenesis of pelagic carbonates from Shatsky Rise, northwest Pacific. *Proceedings of the Ocean Drilling Program: Initial Reports*, *32*, 891–907.

Mettam, C., Zerkle, A. L., Claire, M. W., Izon, G., Junium, C. J., & Twitchett, R. J. (2017). High-frequency fluctuations in redox conditions during the latest Permian mass extinction. *Palaeogeography, Palaeoclimatology, Palaeoecology*, *485*, 210–223. https://doi.org/10.1016/j.palaeo.2017.06.014

Nabbefeld, B., Grice, K., Twitchett, R. J., Summons, R. E., Hays, L., Böttcher, M. E., & Asif, M. (2010). An integrated biomarker, isotopic and palaeoenvironmental study through the Late Permian event at Lusitaniadalen, Spitsbergen. *Earth and Planetary Science Letters*, *291*(1–4), 84–96. https://doi.org/10.1016/j.epsl.2009.12.053

Nielsen, J. K., Shen, Y., Piasecki, S., & Stemmerik, L. (2010). No abrupt change in redox condition caused the end-Permian marine ecosystem collapse in the East Greenland Basin. *Earth and Planetary Science Letters*, *291*(1–4), 32–38.

Payne, J. L., & Clapham, M. E. (2012). End-Permian mass extinction in the oceans: An ancient analog for the twenty-first century? *Annual Review of Earth and Planetary Sciences*, *40*(1), 89–111.

Rennie, V., & Turchyn, A. V. (2014). The preservation of d^{34}SSO$_4$ and d^{18}OSO$_4$ in carbonate-associated sulfate during marine diagenesis: A 25 Myr test case using marine sediments. *Earth and Planetary Science Letters*, *395*, 13–23.

Schrag, D. P., DePaolo, D. J., & Richter, F. M. (1995). Reconstructing past sea surface temperatures: Correcting for diagenesis of bulk marine carbonate. *Geochimica et Cosmochimica Acta*, *59*(11), 2265–2278.

Słowakiewicz, M., Tucker, M. E., Vane, C. H., Harding, R., Collins, A., & Pancost, R. D. (2015). Shale-gas potential of the mid-carboniferous bowland-hodder unit in the Cleveland basin (Yorkshire), central Britain. *Journal of Petroleum Geology*, *38*(1), 59–75. https://doi.org/10.1111/jpg.12598

Stemmerik, L., Bendix-Almgreen, S. E., & Piasecki, S. (2001). The Permian-Triassic boundary in central East Greenland: Past and present views. *Bulletin of the Geological Society of Denmark*, *48*(2), 159–167.

Sun, Y., Joachimski, M. M., Wignall, P. B., Yan, C., Chen, Y., Jiang, H., . . . Lai, X. (2013). Response to Comment on "Lethally hot temperatures during the early Triassic greenhouse." *Science*, *339*(6123), 1033–1033. https://doi.org/10.1126/science.1233090

Surlyk, F., Hurst, J. M., Piasecki, S., Rolle, F., Scholle, P. A., Stemmerik, L., & Thomsen, E. (1986). *The Permian of the Western Margin of the Greenland Sea—A future exploration target* (Vol. 40, pp. 629–659). København, Denmark: Department of Geosciences and Natural Resource Management, University of Copenhagen.

Swart, P. K. (2015). The geochemistry of carbonate diagenesis: The past, present and future. *Sedimentology*, *62*(5), 1233–1304. https://doi.org/10.1111/sed.12205

Thode, H., Monster, J., & Dunford, H. (1961). Sulphur isotope geochemistry. *Geochimica et Cosmochimica Acta*, *25*(3), 159–174.

Twitchett, R. J., Looy, C. V., Morante, R., Visscher, H., & Wignall, P. B. (2001). Rapid and synchronous collapse of marine and terrestrial ecosystems during the end-Permian biotic crisis. *Geology*, *29*(4), 351–354.

Wignall, P. B., & Twitchett, R. J. (2002a). *Extent, duration, and nature of the Permian-Triassic superanoxic event* (Special Paper 356, pp. 395–414). Boulder, CO: Geological Society of America.

Wignall, P. B., & Twitchett, R. J. (2002b). Permian-Triassic sedimentology of Jameson Land, East Greenland: Incised submarine channels in an anoxic basin. *Journal of the Geological Society*, *159*(6), 691–703. https://doi.org/10.1144/0016-764900-120

Wotte, T., Shields-Zhou, G. A., & Strauss, H. (2012). Carbonate-associated sulfate: Experimental comparisons of common extraction methods and recommendations toward a standard analytical protocol. *Chemical Geology*, *326–327*, 132–144.

Zhabina, N., & Volkov, I. (1978). A method of determination of various sulfur compounds in sea sediments and rocks. In *Environmental biogeochemistry and geomicrobiology. Vol. 3: Methods, metals and assessment* (pp. 735–746). Ann Arbor, MI: Ann Arbor Science.

Ziegler, A. M. (1990). Phytogeographic patterns and continental configurations during the Permian Period. *Geological Society, London, Memoirs*, *12*(1), 363–379. https://doi.org/10.1144/GSL.MEM.1990.012.01.35